Stepwise-graded LDPE/aluminum composites: RSM-based optimization for enhanced strength and EMI shielding

Smart Materials and Structures

PURPOSE-LED PUBLISHING™

PAPER • **OPEN ACCESS**

Stepwise-graded LDPE/aluminum composites: RSM-based optimization for enhanced strength and EMI shielding

To cite this article: S Rezaei *et al* 2025 *Smart Mater. Struct.* **34** 085003

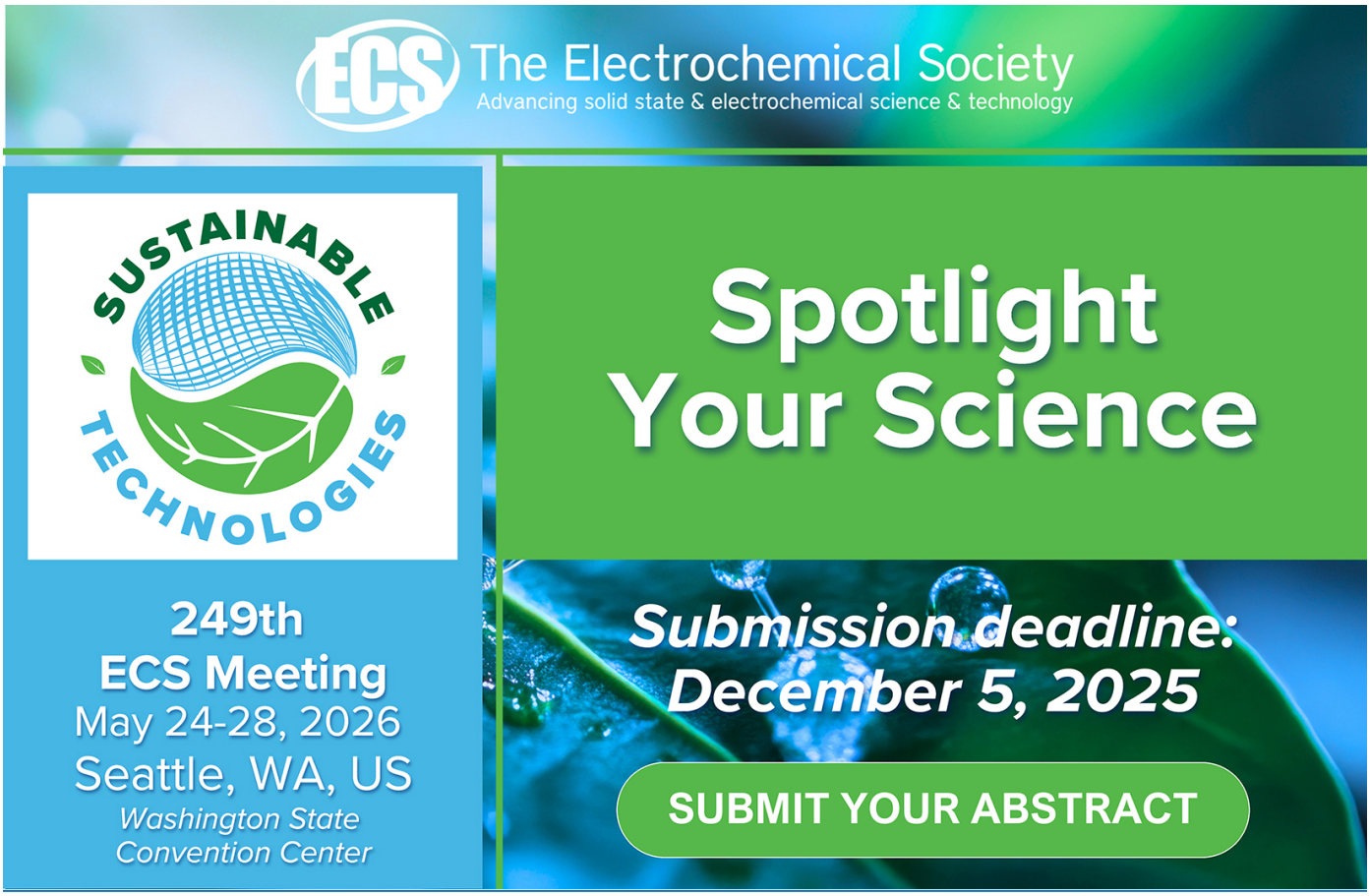

OPEN ACCESS
IOP Publishing
Smart Materials and Structures
Smart Mater. Struct. **34** (2025) 085003 (13pp)
https://doi.org/10.1088/1361-665X/adf308

Stepwise-graded LDPE/aluminum composites: RSM-based optimization for enhanced strength and EMI shielding

S Rezaei[1], **M Mokhtari**[2,*] **and A Askari**[3,4]

[1] Department of Applied Science and Technology, Politecnico di Torino, Corso Duca degli Abruzzi 24, 10129 Turin, Italy
[2] Department of Mechanical Engineering, Technical and Vocational University (TVU), Tehran, Iran
[3] Department of Mechanical Engineering, Ka.C., Islamic Azad University, Karaj, Iran
[4] Manufacturing Engineering and Industrial Technologies, Ka.C., Islamic Azad University, Karaj, Iran

E-mail: m_mokhtari@tvu.ac.ir

Received 27 April 2025, revised 1 July 2025
Accepted for publication 22 July 2025
Published 1 August 2025

Abstract

Among the most salient features of composite materials are lightness, adjustability, and operational manufacturability. In telecommunication structures, it is imperative that the material meet mechanical strength and electromagnetic properties in tandem. Electromagnetic shielding must be considered in telecommunication boxes, in conjunction with structural strength. This article discusses the manufacture and experimental test of polymer multilayers stepwise graded from low-density polyethylene polymer with different percentages of aluminum powder and arrangement. The injection method was employed to manufacture the stepwise graded layers, and the Response surface methodology method was utilized to optimize the powder percentages, arrangements, and identify the optimal percentage for the functional structure layers. A comprehensive review and analysis of the results were conducted to enhance shielding in the frequency range of 1–8 GHz and attain maximum tensile strength. The outcomes demonstrate that the optimal structure attains a tensile strength equivalent to 8.64 MPa, according to the ASTM D 638 standard, and a shielding of −14 dB, in standard waveguide device. The manufacturing process was duly considered, and the obtained results render this structure suitable for utilization in telecommunication applications.

Keywords: stepwise graded, tensile strength, shielding, LDPE, aluminum powder

1. Introduction

The rapid growth of electronic and telecommunication devices has made electromagnetic interference (EMI) a critical issue, leading to potential malfunctions and health risks [1, 2]. Metals like silver, copper, and aluminum have long been used for EMI shielding due to their high conductivity, but their high density, corrosion risk, and limited processability remain key drawbacks [3]. Recently, focus has shifted to environmentally friendly conductive polymer composites (CPCs) with improved processability [4, 5]. While CPCs rely on conductive fillers to form networks, excessive filler content can disrupt impedance matching, increasing wave reflection and environmental impact [6]. Excessive fillers can also reduce the lightweight advantage of CPCs [7]. Researchers are focusing on optimizing filler arrangement to achieve effective EMI shielding with minimal filler content [8].

Conductive fillers are widely studied for enabling EMI-shielding polymer components, with particular focus on metal-based composites using fillers like silver-coated particles and

* Author to whom any correspondence should be addressed.

metal fibers [9]. To enhance shielding while minimizing density, metals are often used as particles or powders dispersed in polymer matrices [10]. Composite polymers filled with metal particles provide advantages such as being lightweight, highly resistant to corrosion, and possessing plasticity [11]. Various research work carried out on using particles are reported in this section. Chou *et al* [12] developed acrylonitrile–butadiene–styrene composites using nickel powder and filaments via melt and dry mixing, showing that dry mixing with 3 vol% filaments yielded a superior shielding effectiveness (SE) of 36 dB, compared to lower SE from 20 vol% powder using melt mixing.

Material synthesis for EMI shielding is advancing rapidly, with ongoing efforts to develop lightweight, strong materials with high SE using alloys and composites containing elements like iron, nickel, aluminum, and magnesium [13]. Aluminum alloys and composites are also used for EMI shielding due to their wide applicability and strong mechanical properties [14].

Despite their effectiveness, metals are limited in EMI shielding applications due to cost and weight. Polymers, preferred for their lightness and flexibility, lack intrinsic EMI shielding because of their insulating nature. This limitation is commonly addressed by embedding conductive fillers into polymer matrices to enhance shielding performance [15, 16]. CPCs offer superior durability, uniformity, and moldability over surface coatings in EMI shielding applications [17]. Unlike metal-based materials, CPCs are increasingly favored for their light weight, corrosion resistance, flexibility, and ease of processing [18]. Research continues to explore polymer blend composites with conductive fillers for EMI shielding. Yuan *et al* studied LDPE and poly (vinylidene fluoride blends with multi-walled carbon nanotubes (MWCNTs), observing improved dielectric properties due to double-percolated structures, where MWCNTs localized in the LDPE phase, enabling superior performance at lower filler content than single-phase LDPE composites [19]. LDPE is a widely used thermoplastic known for its processability, non-toxicity, low-temperature stability, and strong chemical resistance, maintaining its market relevance despite newer alternatives [20].

Optimal EMI shielding requires high conductivity and a well-structured conductive network, relying on multi-interface absorption and hysteresis losses driving increased focus on structural design innovations [21, 22]. EMI shielding materials are classified into four types: uniform, segregated, foamed, and layered structures [4]. With the rise of smart, portable, and wearable electronics, layered configurations are gaining interest due to their lightweight, flexibility, and enhanced multi-interface absorption capabilities [23]. Guo *et al* developed a layer-by-layer graphene-Fe_3O_4 hybrid composite with gradual impedance matching, achieving over 30 dB absorption SE and 10 dB reflection SE at just 300 μm thickness, along with excellent mechanical properties [24, 25].

To enhance EMI shielding in plastics, molders typically use conductive coatings, fillers, or intrinsically conductive polymers. Among these, injection-molded composites with conductive fillers are increasingly favored for their practicality and scalability [26]. Injection molding is widely adopted for its ability to produce complex plastic parts with high precision, low cost, and fast cycle times [27]. Injecting conductive fillers into polymers to produce EMI-shielding materials has gained considerable attention. Studies have explored polymer-metal composites and how injection parameters influence their properties and SE [27, 28].

Functionally graded materials (FGMs) are advanced materials designed with deliberate microscopic variations in composition and structure to achieve specific properties tailored to a desired orientation [29]. FGMs provide designers with customized material behavior and exceptional performance, especially in specialized environments [30]. Microstructural gradation in FGMs enables precise tuning of material properties for specific functions. Compared to single-layer absorbers, FGMs offer improved microwave absorption and broader bandwidth by optimizing layer-wise permittivity and permeability for better impedance matching [31]. The gradient structure in FGMs improves internal reflection attenuation and reduces costs by minimizing reliance on expensive fillers like gold and silver [32, 33]. Thus, multifunctional FGMs are being investigated for electromagnetic noise suppression [34], as demonstrated in a study by Sugano and Takahashi [35], Thus, multifunctional FGMs are being explored for electromagnetic noise suppression. Liu *et al* investigated multilayer graded plates with gradual compositional variation, reporting strong broadband absorption along with reduced thickness and weight.

The evaluation of composite structures with regard to electromagnetic considerations has been previously reviewed by the authors [36, 37]. The advantages and numerical analysis of composite joints considering step-function properties have also been reviewed in other papers [38, 39].

In this article, the shielding properties and strength of LDPE were studied by using aluminum microparticles. The optimal arrangement of step-wise FGM was done using the RSM method in design expert software. The specimens proposed in the test design were produced by the injection method, and the standard tensile test specimens and shielding evaluation were removed from the inside by the machining method. The results of the tests were used to complete the optimization process in RSM, and the optimal final arrangement was proposed with the aim of improving the strength properties of the produced step-wise functional composite and simultaneously improving its shielding properties. Examination of the experimental results shows that both strength and shielding objectives can be achieved. The obtained composites are usable and practical for use in telecommunication and electronic industries, confirming the production method along with the benefits obtained. The SE of the proposed composite was experimentally evaluated across the 1–8 GHz frequency range, which is widely used in microwave, radar, and telecommunication applications.

While many prior studies have focused either on enhancing EMI shielding or improving mechanical performance separately, few have addressed both aspects within a scalable injection molding process using lightweight, cost-effective materials. In this study, we propose a novel, stepwise-graded LDPE/aluminum composite architecture, optimized via RSM,

to simultaneously achieve high SE and tensile strength. This dual-performance strategy fills a critical gap in the current literature on multifunctional polymer-metal composites.

2. Experimental methods

2.1. Materials

This research employed a commercially available pure aluminum powder obtained from Unifine Co., Ltd, with an average particle size of 5.71 μm. Scanning electron microscopy (SEM, Hitachi, SU-6600) revealed the near-spherical shape of the powder particles, which exhibited a broad size range. This morphology contributes to improved moldability [40] and enhances the mechanical properties [41], as depicted in figures 1(a) and (b) presents the corresponding EDX spectrum. It confirms the elemental composition of the powder, displaying a prominent Al Kα peak that verifies the aluminum-rich nature of the material. A minor oxygen signal (O Kα) is also present, which can be attributed to the formation of a thin surface oxide layer—an expected occurrence in aluminum powders due to their high reactivity in ambient conditions. The illustration also indicates occasional agglomeration of the particles, underscoring the importance of ensuring a homogeneous feedstock and dispersing the powder particles effectively within the polymeric binder system. During the injection process, achieving high density and, consequently, superior mechanical properties largely depends on the broad distribution of the powder particles utilized [42]. Hence, the selection of powder particles was aimed at reinforcing these attributes. The particle size distribution of the powder underwent analysis utilizing a laser diffraction particle size analyzer (HORIBA, LA-960), as depicted in figure 2.

The slope parameter (S_w) of the log-normal cumulative distribution was determined for the powder using equation (1) [43]. During injection molding, it is desirable for the S_w value to fall within the range of 2–7. A S_w value near 2 suggests that the powder particle size distribution offers increased viscosity of the feedstock and injection pressure during the molding stage. Conversely, S_w values nearing 7 indicate a narrower particle size distribution, with particles in closer proximity to each other.

$$S_w = \frac{2.56}{\log_{10}\frac{D_{90}}{D_{10}}}. \quad (1)$$

The density of the pycnometer was determined utilizing an automated helium pycnometer (Accupyc 1330, Micromeritics). Both apparent and tap densities were assessed employing a tap density volumeter (BT-300, Bettersize) and the D-values (D_{10}, D_{50}, and D_{90}) represent the points where 10%, 50%, and 90% of the cumulative mass are intercepted. The attributes of the powder are outlined in table 1.

The binder system comprises three distinct constituents: LDPE serving as the backbone polymer, Paraffin Wax acting as a filler to enhance the rheological properties of the feedstock, and Stearic Acid (SA) functioning as a surfactant to augment powder particle wetting with the binder system and provide lubrication during molding. Detailed specifications for each binder component are provided in table 2. The average molecular weight of the binder components was determined using a gel permeation chromatograph analyzer (PL-GPC 200 system).

2.2. Feedstock preparation

Since the aim of this article was to produce a three-layer piece with different percentages of aluminum, feedstocks with 0, 30, and 60% aluminum powder were produced, the details of which are given in table 3. To ensure the desired flowability, it is essential to evenly disperse the optimal amount of powders within the binder system of the feedstock [44]. This approach not only enhances the dimensional stability of the component but also helps prevent localized shrinkage. The compounding process of feedstocks involved utilizing a torque rheometer (Haake PolyLab QC Lab Mixer) to determine the critical solids loading parameters. Mixing was conducted with a barrel temperature of 150 °C, a blade rotational speed of 150 rpm, and a duration of 30 min. Following the application of the optimal solids loading, the feedstock production involved utilizing a twin-screw mixer (KMC-at. The mixing temperature gradient ranged from 145 °C to 160 °C from the hopper to the nozzle until a homogeneous feedstock was attained. In figure 3, the schematic of the feedstock production process is displayed.

2.3. Injection Molding

The HTF60Wll HAITIAN ARAS machine was employed for the injection molding process, In figure 4, the schematic of the device and injection process is shown. For the injection process, we have used a circular mold with a diameter of 16 cm and a thickness of 6 mm, as shown in figure 4. In order to be able to reach a piece with a thickness of 6 mm in three layers, we have used two disk-like plates with thicknesses of 4 and 2 mm. The work process has been such that we first installed the disk with a diameter of 4 mm on the mold, which allows us to inject a 2 mm layer. Then we remove the 4 mm disc from the mold and install the 2 mm disc and put the injected 2 mm plate on it and again a 2 mm space is left which we inject inside, which is the result. An injected 4 mm plate was obtained. Finally, without any disc, we put the injected 4 mm plate into the mold and inject the last layer on it, which finally resulted in a 6 mm plate with different layers. The injection molding parameters are listed in table 4, these values are derived from Rezaei and Askari [45].

To produce the sample, we carried out a limited set of experiments. These experiments were designed using the RSM, specifically employing a three-variable Box–Behnken Design (BBD) with three center points and a quadratic model. The RSM inputs are detailed in table 5.

Given the variation range of the RSM inputs, we utilize the BBD algorithm embedded in the RSM simulation

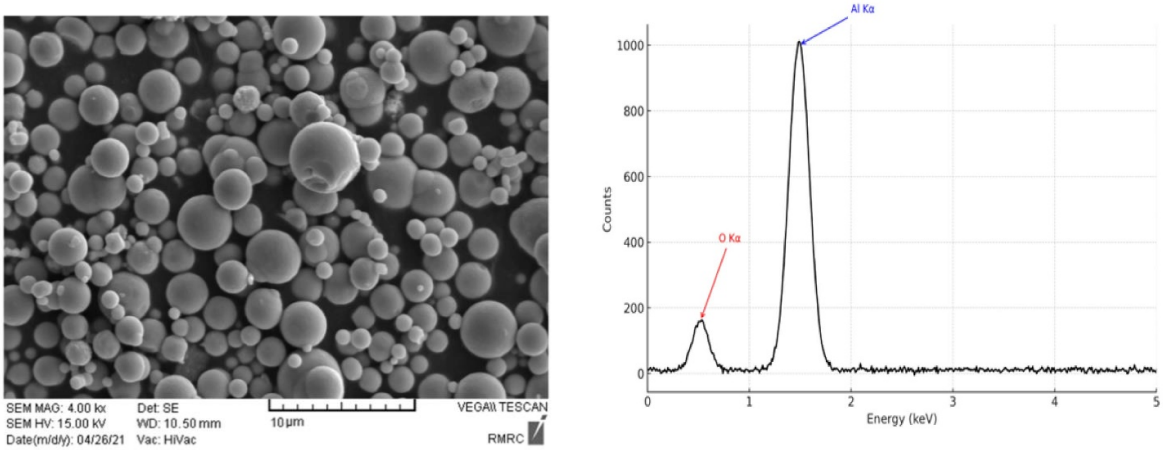

Figure 1. Scanning electron micrograph of the used aluminum gas-atomized powder. (a) SEM micrograph of the gas-atomized aluminum powder showing spherical morphology. (b) EDX spectrum of the same powder, indicating dominant Al Kα and minor O Kα peaks.

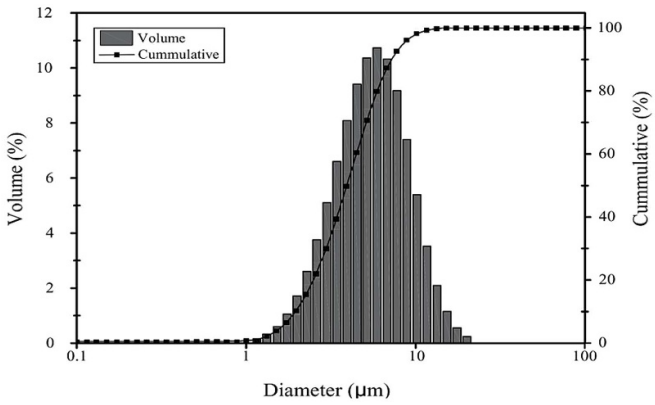

Figure 2. Particle size distribution of the used aluminum powder particles.

Table 1. Characterization of the used aluminum powder particles.

Characteristics	Aluminum powder	
Particle Size (μm)	D_{10}	3.21
	D_{50}	5.71
	D_{90}	8.57
Distribution slope parameter	$S_w = \frac{2.56}{\log_{10}\frac{D_{90}}{D_{10}}}$	4.71
Density (g cm^{-3})	Apparent density	2.75
	Tap density	4.36
	Pycnometer density	7.8423

Table 2. Physical properties of the used binder system components.

Component	Supplier	Density (g cm^{-3})	Average Molecular Weight Mw (g mol^{-1})	Melting temperature ($^\circ$C)	Decomposition temperature ($^\circ$C)
LDPE	Jam Petrochemical Company	0.93	100 000	115	350
Paraffin Wax	Pankaj Impex	0.88	163.31	54.2	436.5
Stearic acid (SA)	Prakash Chemicals	0.94	560	69–72	263–306

Table 3. Determining the specifications of (a) 30 and (b) 60% feed stocks and binders used.

Binder system and powder	Fractional wt.	Density (g cc^{-1})	Mass (g)
	(a)		
Wax	0.575	0.902	2170
PP	0.25	0.9	1507
SA	0.025	0.94	95
Al	1.000	1.250	1810
	(b)		
Wax	0.575	0.902	562
PP	0.25	0.9	391
SA	0.025	0.94	25
Al	1.000	1.250	1813

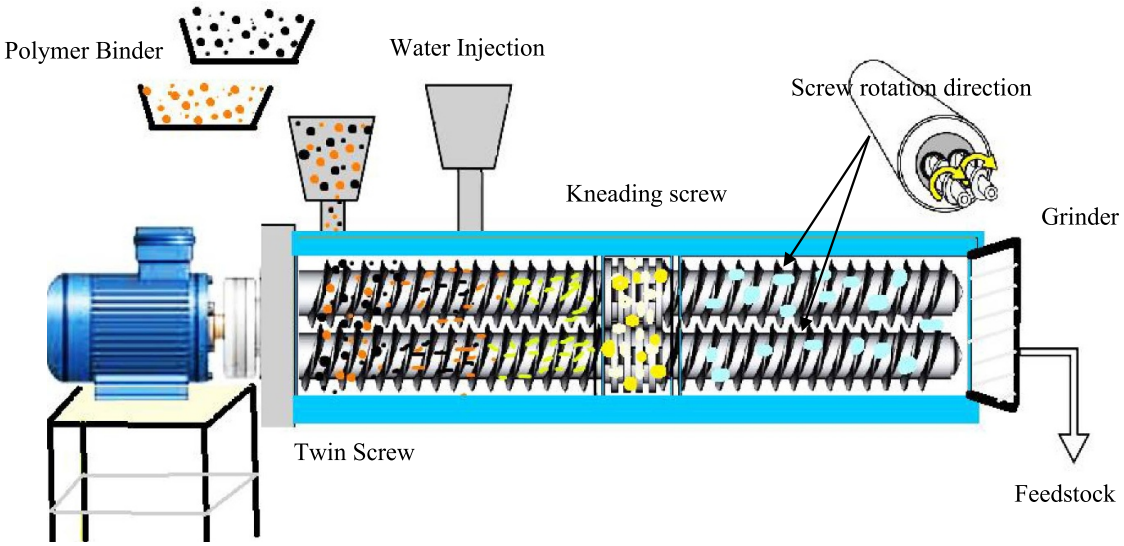

Figure 3. The schematic of a twin-screw mixer.

tool provided by Design Expert 11.0.3.0 (STATEASE Inc., Minneapolis, USA). The model output is set to measure the strength (according to ASTM D634) and shielding based on a standard waveguide measurement. Respectively. Based on the experimental parameters outlined in table 5, running the RSM experimental design logic with the objectives of maximizing strength and shielding led to the definition of 15 experiments, as shown in table 6. Subsequently, the strength and shielding parameters are entered into Design Expert software to identify the optimal settings.

3. Result and discussion

3.1. Optimization of the designed experiments

We discussed that the RSM tool involves 15 experiments, detailed in table 6, which display the actual measurements of strength and shielding. Using the BBD algorithm, we then derive two formulas to express strength and shielding as functions of RSM inputs. Since many factors have only a minor impact on the results, we use analysis of variance to identify the significant parameters. Tables 7 and 8 provide the relevant data, where p-values indicate the significance of model terms; terms with p-values below 0.1 are considered significant. Consequently, for strength, the significant terms include A, B, C, AB, AC, BC, A^2, B^2, and C^2, while for shielding, the significant terms are A, B, and C. The final expressions for strength and shielding are as follows equations (2) and (3):

$$\begin{aligned}\text{Strength} = {} & 8.5 - 0.1325A + 0.61375B - 0.07625C \\ & + 0.4875AB + 0.4925 + AC0.385BC - 0.8125A^2 \\ & - 0.32 - B^2 - 0.825C^2 \end{aligned} \tag{2}$$

$$\text{shielding} = -10.24 - 1.3075A - 1.82625B - 1.31375C. \tag{3}$$

Positive signs in the model terms indicate a synergistic effect, while negative signs denote an antagonistic effect [46].

The Values of measured and predicted strength and shielding values are shown in figure 5, it is clear that the measured values closely align with the predicted ones, suggesting that equations (2) and (3) provide a good approximation for

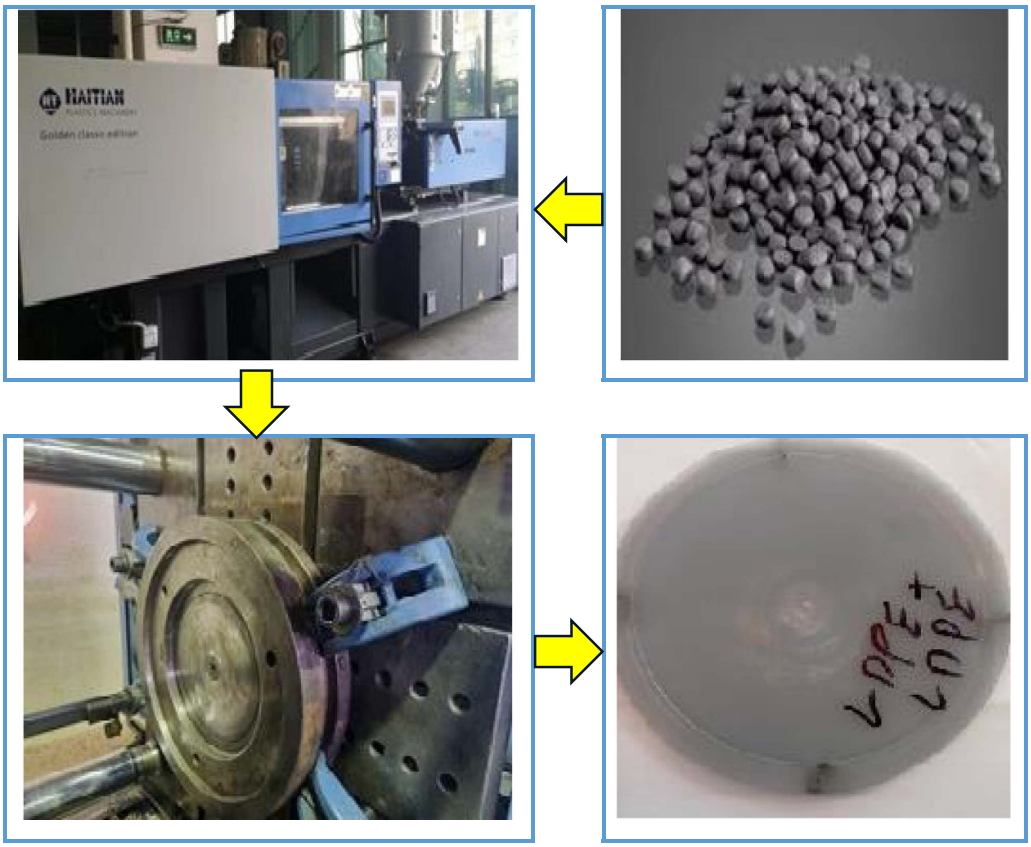

Figure 4. The schematic of the injection process.

Table 4. Injection molding parameters.

Injection temperature (◦C)	Injection speed (mm s^{-1})	Holding pressure (bar)	Holding time (s)	Injection pressure (bar)
155	80	83	9	132

Table 5. The levels of the experimental factors used in the design of experiments (DOE) for RSM modeling.

No	Variable		−1	0	+1
1	*A*	Layer—*A*	0	30	60
2	*B*	Layer—*B*	0	30	60
3	*C*	Layer—*C*	0	30	60

these parameters. However, some deviation is observed in specific cases for SE. This may be attributed to localized particle agglomeration, non-uniform aluminum dispersion, or slight inconsistencies in layer thickness and surface morphology. These factors can alter electromagnetic wave behavior particularly internal reflection and absorption resulting in measured values differing from predictions. Unlike tensile strength, shielding performance is more sensitive to such microstructural and interfacial variations. To verify the validity of the equations, we use the R^2 value, which represents the ratio of the sum of squares due to regression to the total sum of squares. An R^2 value of 1 would signify a perfect fit, indicating that the model's predictions match the experimental results very well [47]. The Predicted R^2 for strength and shielding aligns reasonably with the Adjusted R^2, with a difference of less than 0.2. This indicates that the approximations for strength and shielding are valid, as the variance of errors is smaller compared to the variance of the dependent variables. Detailed data supporting this analysis can be found in tables 9 and 10.

Having validated the expressions for strength and shielding, we now use equations (2) and (3) to determine the optimal percentage of aluminum in the layers to maximize strength and minimize shielding. The resulting optimal parameter values are listed in table 11. Based on these parameters, the fabrication process was carried out once more, resulting in the final sample. The measured strength and shielding of this sample were found to be 8.97 (MPa) and −14.628 (dB) respectively.

Table 6. 15 designed tests via the Box–Behnken technique, together with their experimental and predicted values of the injected parts strength and shielding.

Test number	*A*:%AL In the first Layer	*B*:%AL In the second Layer	*C*:%AL In the third Layer	Measured strength	Predicted Strength	Measured shielding	Predicted shielding	% Error (Strength) based on experiment result	% Error (Shieldin) based on experiment result
1	0	0	30	7.25	7.33	−6.9	−7.1	2.07	2.42
2	60	0	30	6.26	6.13	−9.49	−9.72	1.73	12.31
3	0	60	30	7.5	7.63	−12.26	−10.75	1.41	20.77
4	60	60	30	8.46	8.34	−11.07	−13.37	0.65	3.67
5	0	30	0	7.61	7.56	−7.34	−7.61	3.27	7.83
6	60	30	0	6.11	6.31	−11.1	−10.23	3.01	8.65
7	0	30	60	6.63	6.43	−11.21	−10.24	0.70	22.10
8	60	30	60	7.1	7.15	−16.51	−12.86	1.09	6.60
9	30	0	0	7.28	7.20	−6.66	−7.10	1.03	13.44
10	30	60	0	7.74	7.66	−12.42	−10.75	1.29	5.65
11	30	0	60	6.2	6.28	−9.2	−9.72	23.41	20.43
12	30	60	60	8.2	6.28	−11.11	−13.38	23.41	20.4
13	30	30	30	8.25	8.5	−9.42	−10.24	3.03	8.7
14	30	30	30	8.4	8.5	−9.48	−10.24	1.19	8.01
15	30	30	30	8.5	8.5	−9.32	−10.24	0	9.87

Table 7. Analysis of variance of regression coefficients of models for strength.

Source	Sum of Squares	df	Mean Square	*F*-value	*p*-value	
Model	10.47	9	1.16	33.29	0.0006	significant
A-%AL in the first layer	0.1405	1	0.1405	4.02	0.1012	
B-%AL in the second layer	3.01	1	3.01	86.29	0.0002	
C-%AL in the third layer	0.0465	1	0.0465	1.33	0.3006	
AB	0.9506	1	0.9506	27.22	0.0034	
AC	0.9702	1	0.9702	27.78	0.0033	
BC	0.5929	1	0.5929	16.98	0.0092	
A^2	2.44	1	2.44	69.79	0.0004	
B^2	0.3781	1	0.3781	10.83	0.0217	
C^2	2.51	1	2.51	71.96	0.0004	
Residual	0.1746	5	0.0349			
Lack of Fit	0.1746	3	0.0582			
Pure Error	0.0000	2	0.0000			
Cor Total	10.64	14				

Table 8. Analysis of variance of regression coefficients of models for shielding.

Source	Sum of Squares	df	Mean Square	*F*-value	*p*-value	
Model	54.17	3	18.06	5.99	0.0113	significant
A-%AL in the first layer	13.68	1	13.68	4.54	0.0565	
B-%AL in the second layer	26.68	1	26.68	8.85	0.0126	
C-%AL in the third layer	13.81	1	13.81	4.58	0.0556	
Residual	33.15	11	3.01			
Lack of Fit	33.15	9	3.68			
Pure Error	0.0000	2	0.0000			
Cor Total	87.31	14				

3.2. Strength of the specimens

As illustrated in figure 6, it depicts the interaction effect of the aluminum percentage in the three layers on strength. In figures 6(a) and (b), it is evident that a moderate percentage of aluminum powder in the first layer leads to an increase in strength. A similar trend is observed in the third layer, as shown in figures 6(b) and (c). However, the behavior differs for the second layer. In figures 6(a) and (c), we observe a significant increase in strength as the aluminum powder percentage in the second layer rises. This is due to the fact that the addition of metal particles makes the material more brittle

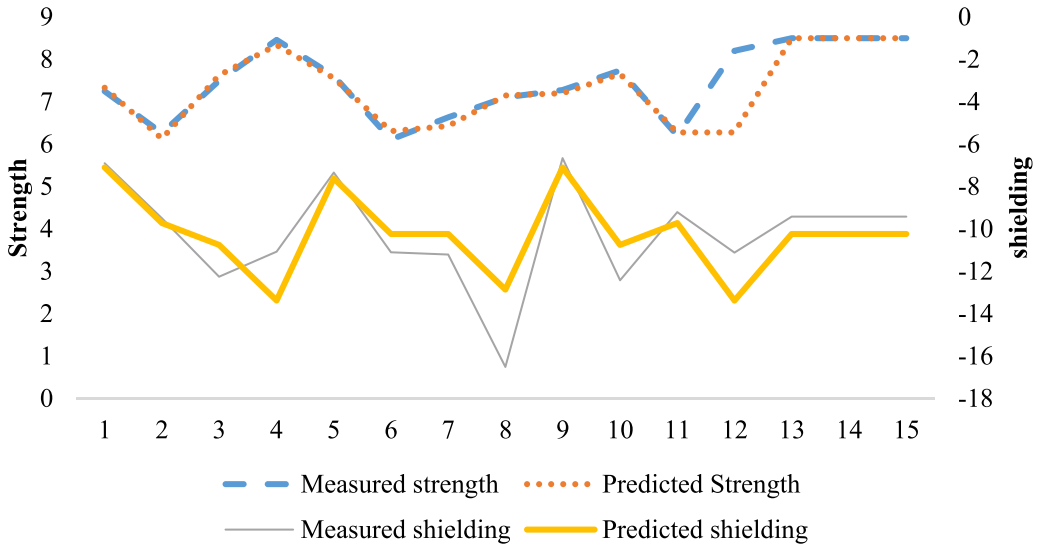

Figure 5. The values of measured and predicted strength and shielding.

Table 9. The R^2 values for the strength equation.

Std. Dev.	0.1869	R^2	0.9836
Mean	7.46	Adjusted R^2	0.9540
C.V. %	2.51	Predicted R^2	0.8874
		Adeq precision	15.5074

Table 10. The R^2 values for the shielding equation.

Std. Dev.	1.74	R^2	0.6203
Mean	−10.24	Adjusted R^2	0.5168
C.V. %	16.96	Predicted R^2	0.3190
		Adeq precision	7.0054

Table 11. Optimum percentage of aluminum in the layers for maximize strength and minimize shielding.

%AL of the layer *A*	%AL of the layer *B*	%AL of the layer *C*	Strength	Shielding	Desirability
53.008	60.000	52.113	8.646	−14.033	0.469

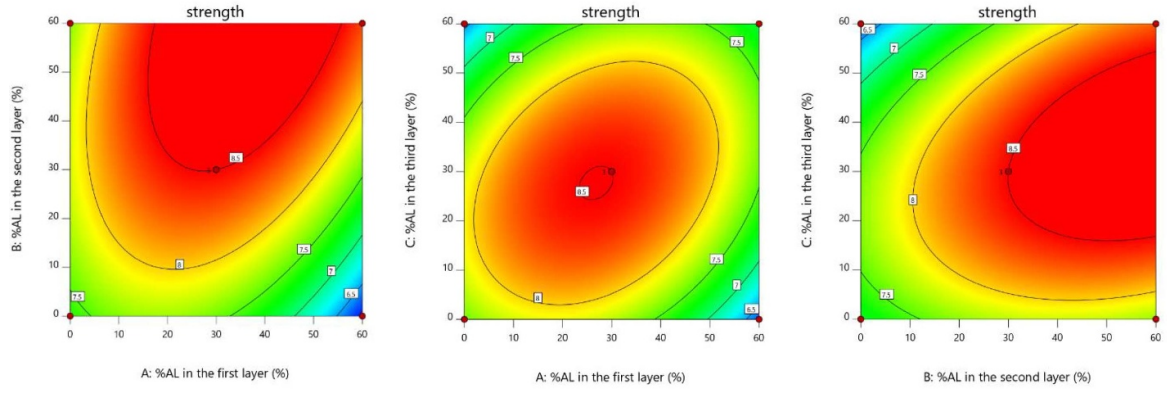

(a) (b) (c)

Figure 6. Strength contour plot of two mutual parameters: variation with aluminum content in three layers.

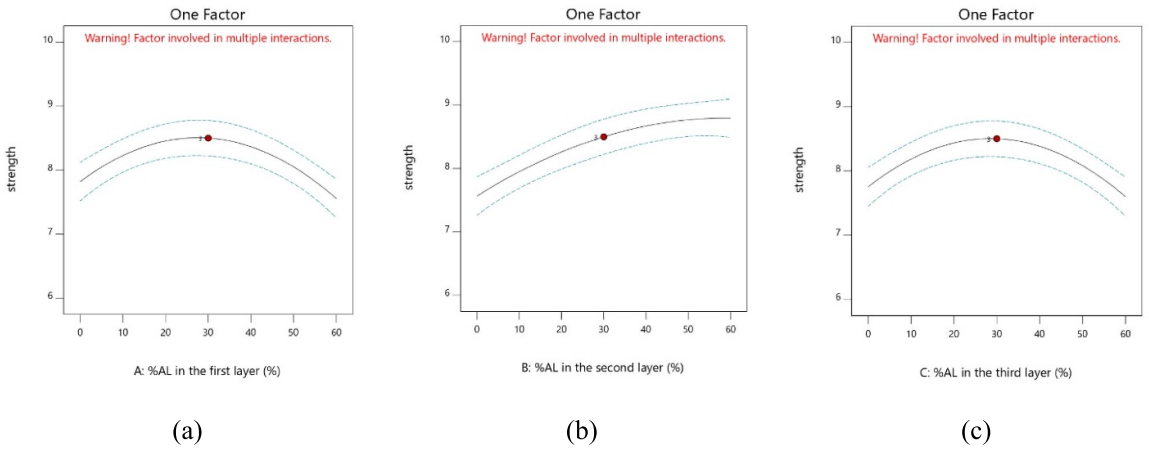

Figure 7. Strength response to a single factor: aluminum content in the three layers.

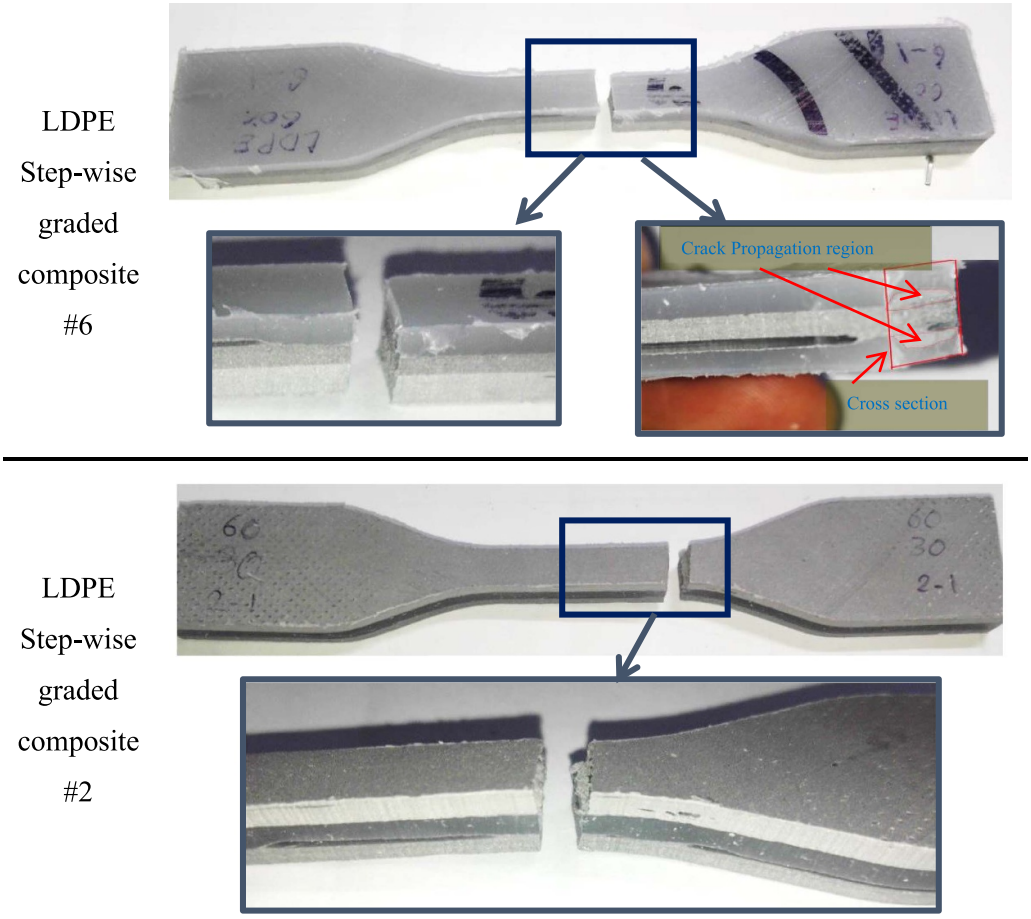

Figure 8. Tensile samples of step-wise graded LDPE composite and damaged region during tensile test.

and increases its modulus of elasticity. In other words, the composite sample with added metal powder exhibits smaller elongation but a higher elastic modulus. Using this layer in the middle of the structure enhances the overall load tolerance of the entire layers. Additionally, the stress distribution across the thickness becomes more uniform. Meanwhile, the layers on the outer sides experience more elongation, transferring the primary load through shape changes, while the middle layer, with its higher modulus, acts as a retaining core. This combination leads to a higher strength overall [48, 49]. Figure 7 illustrates the independent effects of aluminum percentage in each layer on material strength. The effect of aluminum percentage on material strength varies across different layers. In the figures 7(a) and (c), strength follows a parabolic

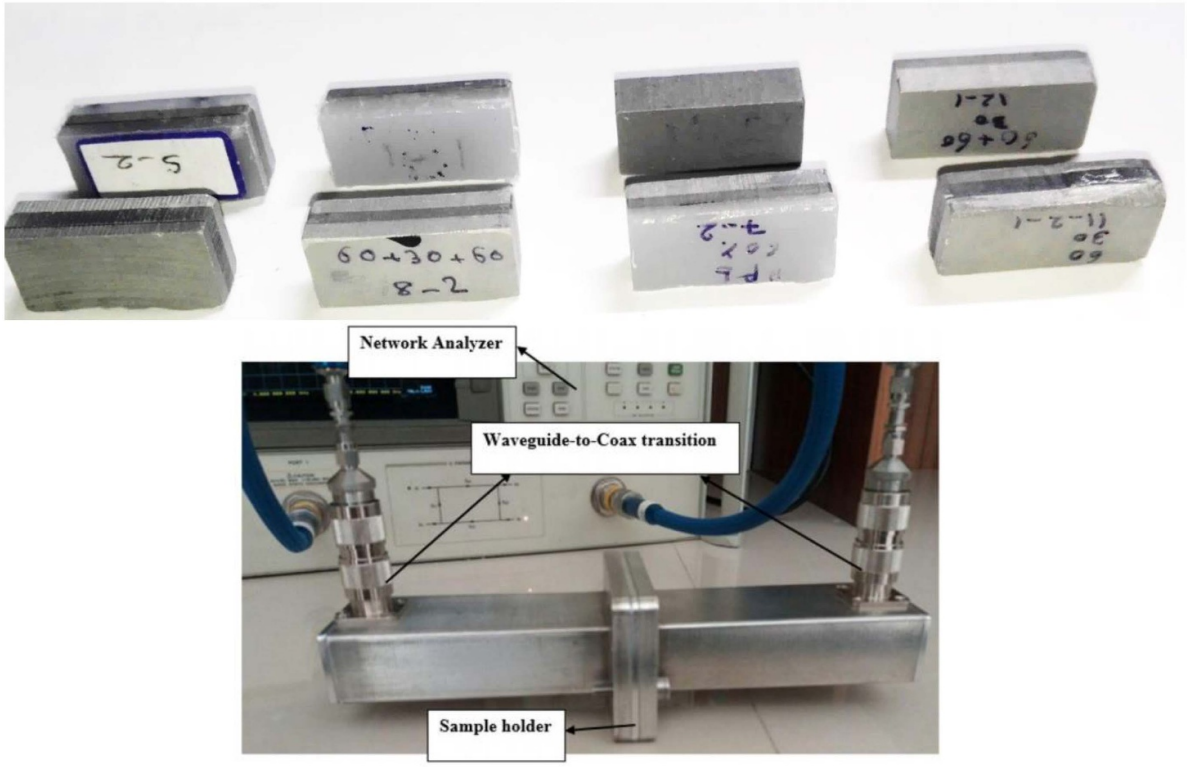

Figure 9. Some shielding test samples of step-wise graded LDPE in the range of 1–8 GHz.

trend, meaning there is an optimal aluminum content beyond which strength decreases, likely due to structural defects or phase transformations. However, in the figure 7(b) layer, strength continuously increases with more aluminum, suggesting it plays a reinforcing role in the material. These differences arise due to stress distribution, microstructural changes, and bonding effects between layers. Therefore, optimizing the aluminum content in each layer is crucial for achieving maximum strength and stability [50].

In order to ascertain the tensile strength of the samples under consideration, the samples were fabricated in accordance with the previously described method and the ASTM standard dimensions were used for tensile strength testing. The tensile test was repeated twice for each condition and the results were averaged and reported. Figure 8 shows an example of the fabricated and tested composites. As illustrated in the detailed view, the fracture zone was determined by the brittleness and softness of the structure, influenced by the stepped nature of the properties. In brittle areas, the crack exhibited rapid growth, while in soft areas, with matrix elongation, the joint area underwent significant deformation. The test design investigated the interaction between brittle and soft structures and the variation in the percentage of aluminum particles. Figure 8 Tensile samples of step-wise graded LDPE composite and damaged region during tensile test.

3.3. Shielding of the specimens

In the interaction between structures and electromagnetic waves, three behaviors are observed: absorption, reflection, and transmission [51]. The degree of shielding is determined by the inability to find the passage of electromagnetic waves through the fabricated layers. An X-band waveguide was used to evaluate this parameter, with the fabricated sample placed in the waveguide by repeating two samples of each arrangement. The parameter related to the passage of waves in the frequency band of 1–8 GHz was studied. As illustrated in figure 9, the test arrangement is depicted schematically. The results of the shielding test are reported in table 6. The use of aluminum metal particles has been shown to increase the absorption and reflection of waves due to their metallic nature. In this test, the use of layered and step-wise functional combinations has been investigated and reported. As illustrated in figure 10, an increase in the aluminum powder content within the structure leads to a decrease in shielding, thereby enhancing its SE. Metal particles can reflect and absorb electromagnetic waves, and this capability increases as the percentage of aluminum powder rises. Additionally, various arrangements have been employed to enhance internal reflections and secondary absorptions, resulting in greater overall absorption and reflection of electromagnetic waves [52].

Considering that most EMI shielding applications benefit from thin and laminar configurations, it is important to evaluate the adaptability of the proposed stepwise-graded LDPE/Aluminum composite to such geometries. Although the present study utilized injection molding to fabricate 6 mm-thick multilayer specimens, the process is inherently compatible with laminar structures. By adjusting mold dimensions and optimizing injection parameters such as temperature, pressure, and holding time, it is feasible to manufacture

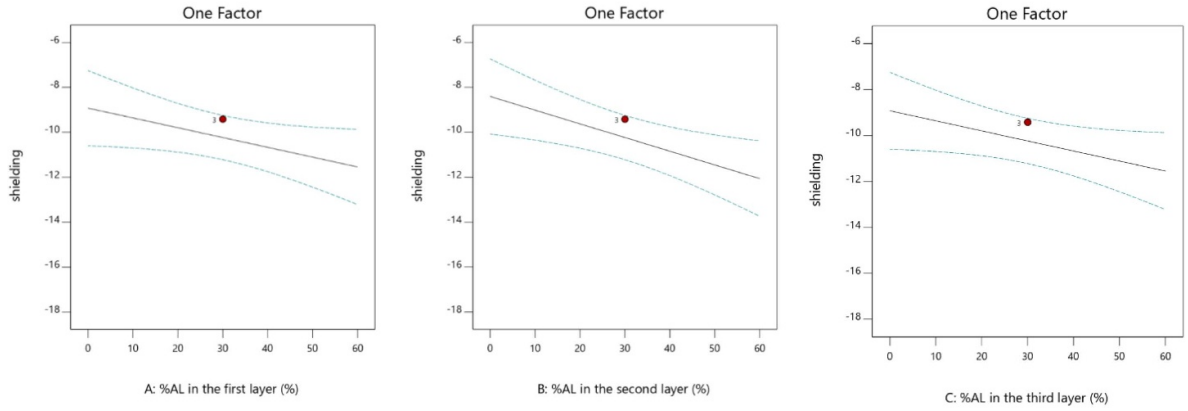

(a) (b) (c)

Figure 10. Shielding response to a single factor: aluminum content in the three layers.

thinner variants of the same composite. Additionally, the selected binder system, consisting of LDPE, paraffin wax, and stearic acid, exhibits high flowability and homogeneity, allowing for effective dispersion of aluminum particles even in reduced thicknesses. The presence of well-distributed metallic particles in the layered structure would continue to support shielding functionality by enabling effective reflection and absorption mechanisms within a thinner profile. Therefore, the developed composite is not only structurally sound in thicker forms but also holds promise for adaptation in practical EMI shielding components with laminar geometries.

Based on RSM modeling, the optimized SE and tensile strength of the composite were predicted to be−14.03 dB and 8.65 MPa, respectively. Although these values are substantially lower than those of pure aluminum metal (50–60 dB SE and 90–150 MPa tensile strength), the composite system offers advantages in weight reduction, ease of processing, and suitability for polymer-based manufacturing techniques. These trade-offs are relevant in applications where full metallic shielding is not feasible or necessary, and where design flexibility and cost are prioritized.

4. Conclusion

FGM composite structures have the potential for wide application in various industries, contingent upon their operational viability. The necessity for two simultaneous properties, in conjunction with the location-based nature of the properties, underscores the imperative for the utilization of functional structures. This paper presents an experimental investigation into the fabrication of an FGM composite derived from LDPE and aluminum powder, with the objective of examining multilayer injectable structures. The experimental cases under consideration were all constrained by operational and manufacturing factors and are in full compliance with the production method. The experimental findings demonstrated that the adhesion of the distinct layers during injection was successful, ensuring the reliability of the method for extensive application in industry. The study investigated two concurrent parameters, strength and electromagnetic shielding. The estimated maximum strengths and shielding for the optimal table 11 were 8.646 MPa and −14.033 dB, respectively. The experimental design and layout selection were methodically executed through the utilization of the RSM approach, facilitating the identification of the optimal structure through a series of 15 experimental tests. The outcomes of these tests substantiated the predicted maximum strength and concurrent shielding capabilities. The proposed structure is poised to serve as a resilient telecommunications framework, exhibiting substantial resistance to radio interference.

Data availability statement

The data cannot be made publicly available upon publication because no suitable repository exists for hosting data in this field of study. The data that support the findings of this study are available upon reasonable request from the authors.

ORCID iDs

S Rezaei 0009-0007-1602-1817
M Mokhtari 0000-0002-3816-2975

References

[1] Shahzad F, Alhabeb M, Hatter C B, Anasori B, Hong S M, Koo C M and Gogotsi Y 2016 Electromagnetic interference shielding with 2D transition metal carbides (MXenes) *Science* **353** 1137–40
[2] Wang H, Ma N, Yan Z, Deng L, He J, Hou Y, Jiang Y and Yu G 2015 Cobalt/polypyrrole nanocomposites with controllable electromagnetic properties *Nanoscale* **7** 7189–96
[3] Lee S H, Kim J Y, Koo C M and Kim W N 2017 Effects of processing methods on the electrical conductivity, electromagnetic parameters, and EMI shielding effectiveness of polypropylene/nickel-coated carbon fiber composites *Macromol. Res.* **25** 936–43

[4] Yao Y, Jin S, Zou H, Li L, Ma X, Lv G, Gao F, Lv X and Shu Q 2021 Polymer-based lightweight materials for electromagnetic interference shielding: a review *J. Mater. Sci.* **56** 6549–80

[5] Wang G *et al* 2020 Influence of the filler dimensionality on the electrical, mechanical and electromagnetic shielding properties of isoprene rubber-based flexible conductive composites *Compos. Commun.* **21** 100417

[6] Zhang H, Zhang G, Li J, Fan X, Jing Z, Li J and Shi X 2017 Lightweight, multifunctional microcellular PMMA/Fe_3O_4@MWCNTs nanocomposite foams with efficient electromagnetic interference shielding *Composites A* **100** 128–38

[7] Shahapurkar K *et al* 2022 Comprehensive review on polymer composites as electromagnetic interference shielding materials *Polym. Polym. Compos.* **30** 09673911221102127

[8] Ju J, Kuang T, Ke X, Zeng M, Chen Z, Zhang S and Peng X 2020 Lightweight multifunctional polypropylene/carbon nanotubes/carbon black nanocomposite foams with segregated structure, ultralow percolation threshold and enhanced electromagnetic interference shielding performance *Compos. Sci. Technol.* **193** 108116

[9] Khushnood R A, Ahmad S, Savi P, Tulliani J-M, Giorcelli M and Ferro G A 2015 Improvement in electromagnetic interference shielding effectiveness of cement composites using carbonaceous nano/micro inerts *Constr. Build. Mater.* **85** 208–16

[10] Krishnasamy J, Thilagavathi G, Alagirusamy R and Das A 2019 Metal-embedded matrices for EMI shielding *Materials for Potential EMI Shielding Applications* (Elsevier) (https://doi.org/10.1016/B978-0-12-817590-3.00007-5)

[11] Los P, Lukomska A and Jeziorska R 2016 Metal-polymer composites for electromagnetic interference shielding applications *Polimery* **61** 663–9

[12] Chou K S, Huang K C and Shih Z H 2005 Effect of mixing process on electromagnetic interference shielding effectiveness of nickel/acrylonitrile-butadiene-styrene composites *J. Appl. Polym. Sci.* **97** 128–35

[13] Pandey R, Tekumalla S and Gupta M 2019 EMI shielding of metals, alloys, and composites *Materials for Potential EMI Shielding Applications* (Elsevier) (https://doi.org/10.1016/B978-0-12-817590-3.00021-X)

[14] Zhang Y, Zhang B, Li K, Zhao G L and Guo S M 2018 Electromagnetic interference shielding effectiveness of high entropy AlCoCrFeNi alloy powder laden composites *J. Alloys Compd.* **734** 220–8

[15] Chiang W Y and Cheng K Y 1997 Processing conditions for electromagnetic interference shielding effectiveness and mechanical properties of acrylonitrile-butadiene-styrene based composites *Polym. Compos.* **18** 748–56

[16] Sawai P and Banerjee S 2008 Electromagnetic interference shielding effectiveness of graphite-filled polypropylene and poly(ether imide) based composites *J. Appl. Polym. Sci.* **109** 2054–63

[17] Zhang W, Dehghani-Sanij A A and Blackburn R S 2007 Carbon based conductive polymer composites *J. Mater. Sci.* **42** 3408–18

[18] Yavuz Ö, Ram M K and Aldissi M 2007 Electromagnetic applications of conducting and nanocomposite materials *The New Frontiers of Organic and Composite Nanotechnology* (Elsevier) (https://doi.org/10.1016/B978-008045052-0.50011-7)

[19] Yuan J-K, Yao S-H, Sylvestre A and Bai J 2012 Biphasic polymer blends containing carbon nanotubes: heterogeneous nanotube distribution and its influence on the dielectric properties *J. Phys. Chem. C* **116** 2051–8

[20] Luo X, Gelves G A, Sundararaj U and Luo J-L 2013 Silver-coated copper nanowires with improved anti-oxidation property as conductive fillers in low-density polyethylene *Can. J. Chem. Eng.* **91** 630–7

[21] Lee S, Jo I, Kang S, Jang B, Moon J, Park J B, Lee S, Rho S, Kim Y and Hong B H 2017 Smart contact lenses with graphene coating for electromagnetic interference shielding and dehydration protection *ACS Nano* **11** 5318–24

[22] Arief I, Biswas S and Bose S 2017 FeCo-anchored reduced graphene oxide framework-based soft composites containing carbon nanotubes as highly efficient microwave absorbers with excellent heat dissipation ability *ACS Appl. Mater. Interfaces* **9** 19202–14

[23] Kumar P, Shahzad F, Hong S M and Koo C M 2016 A flexible sandwich graphene/silver nanowires/graphene thin film for high-performance electromagnetic interference shielding *RSC Adv.* **6** 101283–7

[24] Guo Z, Ren P, Fu B, Ren F, Jin Y and Sun Z 2020 Multi-layered graphene-Fe_3O_4/poly (vinylidene fluoride) hybrid composite films for high-efficient electromagnetic shielding *Polym. Test* **89** 106652

[25] Al-Saleh M H and Sundararaj U 2009 Electromagnetic interference shielding mechanisms of CNT/polymer composites *Carbon* **47** 1738–46

[26] Yang S Y, Chen C Y and Parng S H 2002 Effects of conductive fibers and processing conditions on the electromagnetic shielding effectiveness of injection molded composites *Polym. Compos.* **23** 1003–13

[27] Cheng W S, Chen C S, Chen S C and Chien R D 2009 Investigation of the effects of injection molding processing parameters on conductive polymeric composites for electromagnetic interference shielding effectiveness *Polym. Plast. Technol. Eng.* **48** 216–20

[28] Rezaei S and Askari A 2024 Investigating metal injection molding of 4605 low-alloy steel powder-polymer mixture: parametric optimization of the injection stage using RSM technique *Iran. Polym. J.* **34** 453–64

[29] Naebe M and Shirvanimoghaddam K 2016 Functionally graded materials: a review of fabrication and properties *Appl. Mater. Today* **5** 223–45

[30] Cai Y, Wang N, Cheng L, Yin X, Yin H, Wang Y, Ren X, Li X and Fan X 2019 Electrical conductivity and electromagnetic shielding properties of Ti_3SiC_2/SiC functionally graded materials prepared by positioning impregnation *J. Eur. Ceram. Soc.* **39** 3643–50

[31] Yang R B, Liang W F, Wu C H and Chen C C 2016 Synthesis and microwave absorbing characteristics of functionally graded carbonyl iron/polyurethane composites *AIP Adv.* **6** 055910

[32] Huan C and Wen B 2013 A novel technique for preparation of electrically conductive ABS/Cu polymeric gradient composites *J. Wuhan Univ. Technol. Mater. Sci. Ed.* **28** 1003–7

[33] Vasiraja N, Sathiya Prabhahar R S and Daniel S J 2022 Tensile and flexural characteristic of functionally graded carbon fiber reinforced composites with alumina and yttria stabilized zirconia fillers for bone implant *Mater. Today* **62** 3197–202

[34] Vasiraja N and Nagaraj P 2019 Characterization of SS/Al_2O_3 functionally graded material coating by plasma spray technique on aluminum plate *Mater. Res. Express* **6** 066402

[35] Sugano Y and Takahashi S 2006 Material design of functionally graded plates with function of electromagnetic noise suppression (quantitative evaluation on suppression effect of electromagnetic noise) *Nihon Kikai Gakkai Ronbunshu, A Hen/Trans. Japan Soc. Mech. Eng. A* **72** 1585–92

[36] Nazari F, Taherkhani M, Mokhtari M, Aliakbarian H and Shekoofa O 2020 Efficient design methodology for

sandwich radome panels: a C-band design example *IET Sci. Meas. Technol.* **14** 808–16
[37] Mokhtari M 2024 Development of an electromagnetic compatible composite-insert embedded in a double-curved sandwich panel *J. Sandw. Struct. Mater.* **26** 1509–31
[38] Mokhtari M, Shahravy M and Zabihpoor M 2019 Novel development of dynamic behavior of carbon fiber reinforced polymer sandwich panels with stepwise graded adhesive layer *Aircr. Eng. Aerosp. Technol.* **91** 50–59
[39] Mokhtari M, Shahravi M and Zabihpoor M 2018 Development of dynamic behavior of the novel composite T-joints: numerical and experimental *Adv. Aircr. Spacecr. Sci.* **5** 385
[40] Park S-J, Wu Y, Heaney D F, Zou X, Gai G and German R M 2009 Rheological and thermal debinding behaviors in titanium powder injection molding *Metall. Mater. Trans. A* **40** 215–22
[41] Park D Y, Lee S W, Park S J, Kwon Y-S and Otsuka I 2013 Effects of particle sizes on sintering behavior of 316L stainless steel powder *Metall. Mater. Trans. A* **44** 1508–18
[42] Cambridge University 1990 Aerospace industry is major focus of composites research in Japan *MRS Bull.* **15** 50
[43] Atre S V, Weaver T J and German R M 1998 Injection molding of metals and ceramics *SAE Technical Paper* (https://doi.org/10.4271/982417)
[44] Dhaval M, Sharma S, Dudhat K and Chavda J 2022 Twin-screw extruder in pharmaceutical industry: history, working principle, applications, and marketed products: an in-depth review *J. Pharm. Innov.* **17** 294–318
[45] Rezaei S and Askari A 2024 Moulding of SS316L surgical component using palm-stearin feedstock : rheological analysis, process window and parametric optimisation *Powder Metall.* **67** 246–61
[46] Sahu J N, Acharya J and Meikap B C 2010 Optimization of production conditions for activated carbons from Tamarind wood by zinc chloride using response surface methodology *Bioresour. Technol.* **101** 1974–82
[47] Mehdi H and Mishra R S 2022 An experimental analysis and optimization of process parameters of AA6061 and AA7075 welded joint by TIG+FSP welding using RSM *Adv. Mater. Process. Technol.* **8** 598–620
[48] Jeong C, Hwang S-H, Kim B-J, Chae H G and Bin Park Y 2021 Multilayered composites with modulus gradient for enhanced pressure—temperature sensing performance *Sensors* **21** 4752
[49] Zhang Y, Sun M-J and Zhang D 2012 Designing functionally graded materials with superior load-bearing properties *Acta Biomater.* **8** 1101–8
[50] Evstifeev A, Mavlyutov A, Voropaev A and Volosevich D 2024 Optimization of strength and plasticity in layered aluminum composites through high-pressure torsion treatment *Metals* **14** 1445
[51] Zhou Y, Zhang W, Pan D, Li Z, Zhou B, Huang M, Mi L, Liu C, Feng Y and Shen C 2025 Absorption–reflection–transmission power coefficient guiding gradient distribution of magnetic mxene in layered composites for electromagnetic wave absorption *Nano-Micro. Lett.* **17** 147
[52] Kim T, Do H W, Choi K J, Kim S, Lee M, Kim T, Yu B K, Cheon J, Min B W and Shim W 2021 Layered aluminum for electromagnetic wave absorber with near-zero reflection *Nano Lett.* **21** 1132–40